MOTOROLA LABS

COMPUTATIONAL EME COMPLIANCE ASSESSMENT OF THE XTL5000

UHF MOBILE RADIO, MODEL # M20QTS9PW1AN, FCC ID AZ492FT4870

September 17, 2004 - Revised February 10, 2005

Giorgi Bit-Babik and Antonio Faraone

Motorola Corporate EME Research Lab, Plantation, Florida

Introduction

This report summarizes the computational [numerical modeling] analysis performed to document compliance of the XTL5000 UHF, Model Number M20QTS9PW1AN, Mobile Radio and vehicle-mounted antennas with the Federal Communications Commission (FCC) guidelines for human exposure to radio frequency (RF) emissions. The radio operates in the 380 - 470 MHz frequency band.

This computational analysis supplements the measurements conducted to evaluate the FCC *maximum permissible exposure* (MPE) limits for this mobile device. All test conditions (19 in total) that did not conform with applicable MPE limits were subdivided into two groups — bystander exposures and passenger exposures — and analyzed to determine whether those conditions complied with the *specific absorption rate* (SAR) limits for general public exposure (1.6 W/kg averaged over 1 gram of tissue and 0.08 W/kg averaged over the whole body) set forth in FCC guidelines, which are based on the IEEE C95.1-1999 standard [1]. For both groups, a commercial code based on Finite-Difference-Time-Domain (FDTD) methodology was employed to carry out the computational analysis. It is well established and recognized within the scientific community that SAR is the primary dosimetric quantity used to evaluate the human body's absorption of RF energy and that MPEs are in fact derived from SAR. Accordingly, the SAR computations provide a scientifically valid and more accurate estimate of human exposure to RF energy.

Method

The simulation code employed is XFDTD™ v5.3, by Remcom Inc., State College, PA. This computational suite features a heterogeneous full body standing model (High Fidelity Body Mesh), derived from the so-called Visible Human [2], discretized in 5 mm voxels. The dielectric properties of 23 body tissues are automatically assigned by XFDTD™ at any specific frequency. The "seated" man model was obtained from the standing model by modifying the articulation angles at the hips and the knees. Details of the computational method and model are provided in the Appendix to this report, following the structure outlined in Appendix B.III of the Supplement C to the FCC OET Bulletin 65.

The car model has been imported into XFDTD™ from the CAD file of a sedan car having dimensions 4.98 m (L) x 1.85 m (W) x 1.18 m (H), and discretized in 5mm voxels. For trunk mounted antennas, the wheels and part of the hood were omitted in order to fit within the computational memory (3 GB) available. For roof mounted antennas, part of the trunk had to be removed while maintaining the integrity of the roof connection with the car body. These omissions would not be expected to affect the exposure calculations in any event.

For bystander exposure, the antenna position is 26 cm from the end of the trunk, so as to replicate the experimental conditions used in MPE measurements. For passenger exposure, the distance of trunk mounted antennas from the passenger head was set at 85 cm, so as to replicate the experimental conditions used in MPE measurements. Figures 1 shows one of the XFDTD™ computational models used for bystander exposure. Figures 2 shows one of the XFDTD™ computational models used for passenger exposure to trunk mounted antenna.
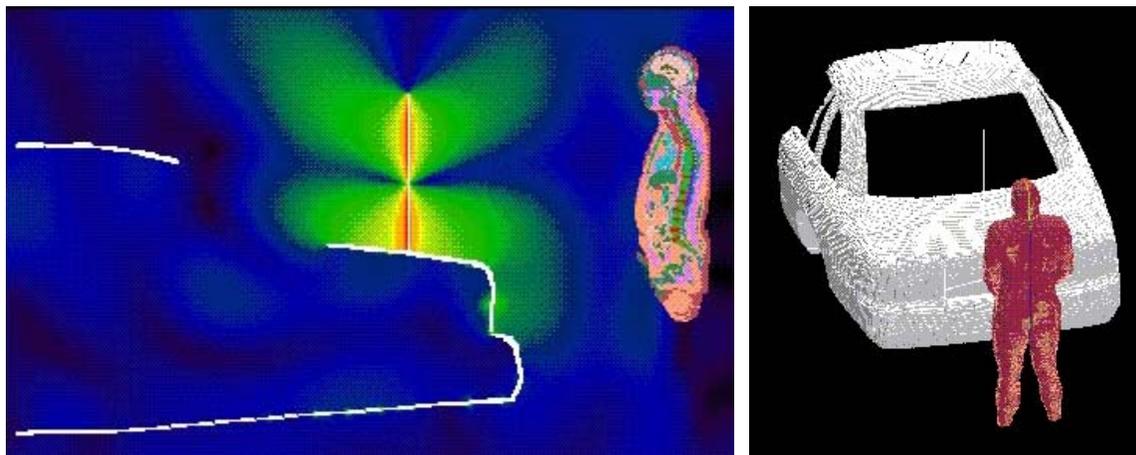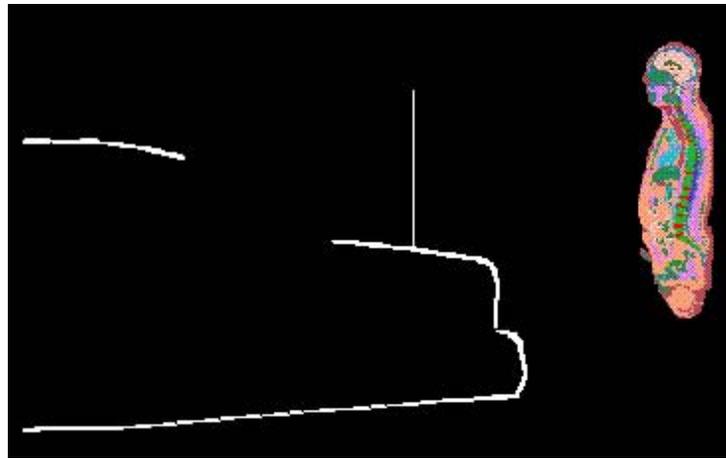
Figure 1: Bystander model exposed to a trunk-mount gain antenna (63.5 cm) operating at 380 MHz: XFDTD geometry, H-field and SAR distribution. The antenna is mounted in the center of the trunk.
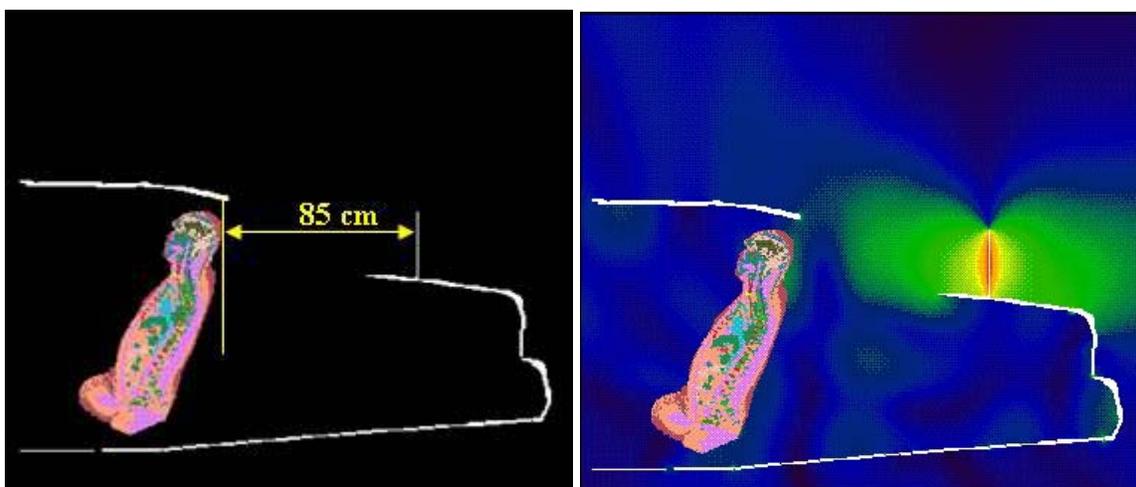

Figure 2: Passenger model exposed to a trunk-mount antenna (29 cm) operating at 470 MHz: XFDTD geometry and H-field distribution. The antenna is mounted at 85 cm from the passenger.

The computational code employs a time-harmonic excitation to produce a steady state electromagnetic field in the exposed body. Subsequently, the corresponding SAR distribution is automatically processed in order to determine the whole-body and 1-g average SAR. The product maximum output power is 120 W rms. Since the ohmic losses in the cable and in the car materials, as well as the mismatch losses at the antenna feed-point, are neglected, and source-based time averaging (50% talk time) is employed, all computational results are normalized to half of it, i.e., 60 W *rms* net output power.

Results of SAR computations for bystanders

The test conditions requiring SAR computations are summarized in Tables I, together with other relevant information and the SAR results. With trunk mount antennas, the bystander is placed next to the trunk of the car, straight back, at 45 degrees from the longitudinal car centerline, and at 90 degrees from it, at a distance of 90 cm from the antenna while maintaining at least 20 cm from the vehicle body, so as to replicate the conditions used in MPE measurements. Twelve cases of bystander - facing towards to or away from the car - were simulated individually.

Table I: Results of the SAR computations for bystander exposure (50% talk-time) behind the car at a separation distance of 90 cm from the trunk-mount antenna while maintaining at least 20 cm from the vehicle body.

MPE Table #	Antenna Kit #	Antenna length		Freq [MHz]	Bystander exposure	Exposure angle	SAR [W/kg]	
		Physical	XFDTD				1-g	WB
29	HAE6013A	29 cm	29 cm	425	Front	0 deg	1.00	0.021
29	HAE6013A	29 cm	29 cm	425	Back	0 deg	0.66	0.023
35	HAE6013A	29 cm	29 cm	425	Front	45 deg	1.03	0.024
35	HAE6013A	29 cm	29 cm	425	Back	45 deg	0.72	0.025
39	HAE6013A	29 cm	29 cm	425	Front	90 deg	0.99	0.015
39	HAE6013A	29 cm	29 cm	425	Back	90 deg	0.55	0.016
49	HAE6013A	29 cm	29 cm	380	Front	45 deg	0.87	0.024
49	HAE6013A	29 cm	29 cm	380	Back	45 deg	0.95	0.025
51	HAE6013A	29 cm	29 cm	470	Front	45 deg	0.93	0.021
51	HAE6013A	29 cm	29 cm	470	Back	45 deg	0.69	0.021
53	HAE6010A	63.5 cm	63.5 cm	380	Front	45 deg	0.89	0.019
53	HAE6010A	63.5 cm	63.5 cm	380	Back	45 deg	0.54	0.020

The SAR distribution for the exposure condition (425 MHz, bystander at 45 degrees facing the car, trunk-mount HAE6013A antenna) that produced the highest peak 1-g SAR average is shown in Fig. 3.

The SAR distribution for the exposure condition (380 MHz, bystander at 45 degrees facing back to the car, trunk-mount HAE6013A antenna) that produced the highest whole body SAR average is shown in Fig. 4.

The overall maximum peak 1-g SAR is 1.03 W/kg, less than the 1.6 W/kg limit, while the maximum whole-body average SAR is 0.025 W/kg, less than the 0.08 W/kg limit.
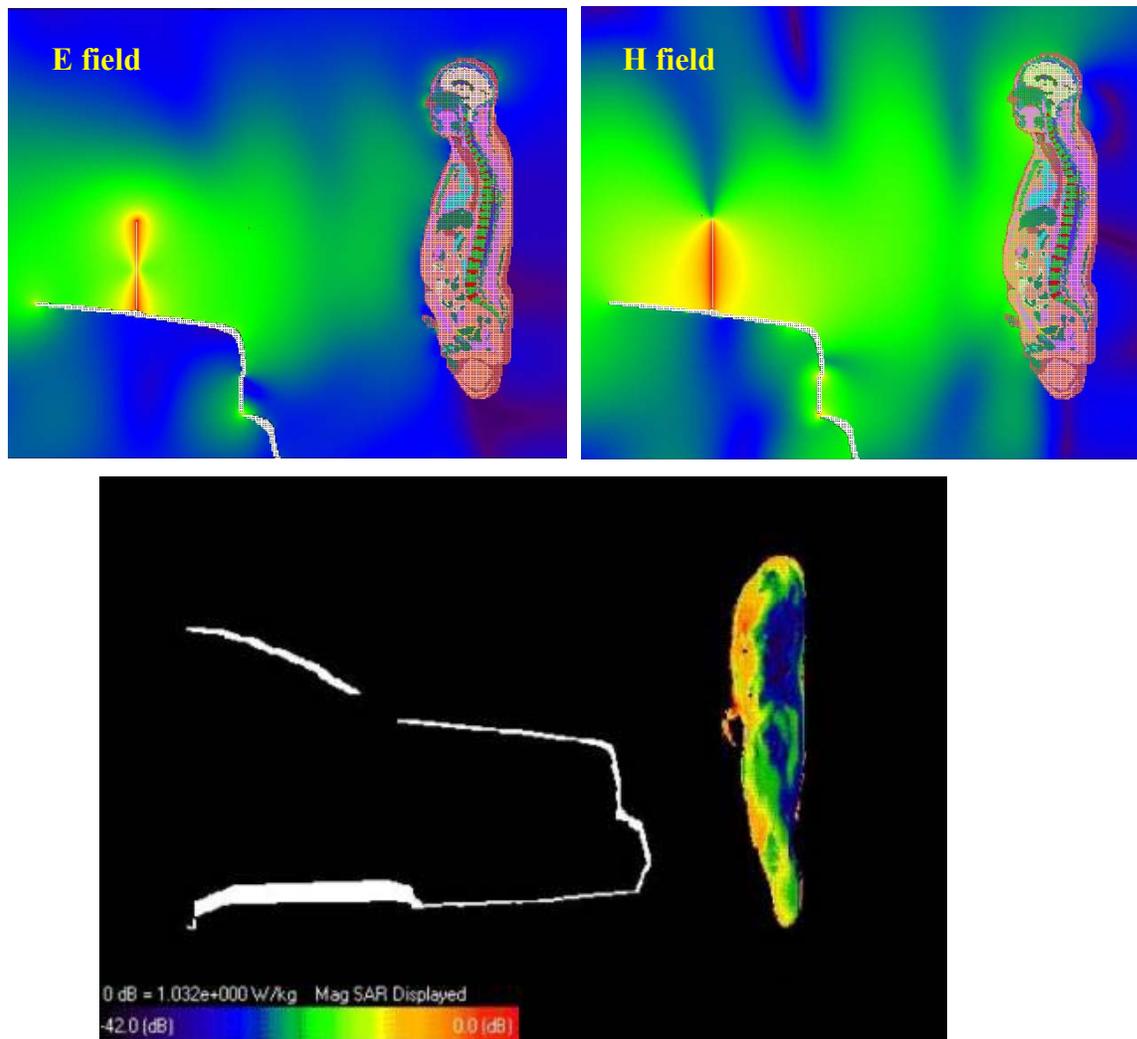

Figure 3. SAR and field distribution at 425 MHz for the bystander at 90 cm from the HAE6013A antenna, placed in the center of the trunk, when facing the car at 45 degrees. The SAR contour plot in the figure is relative to the plane where the peak 1-g average SAR for this exposure condition occurs.
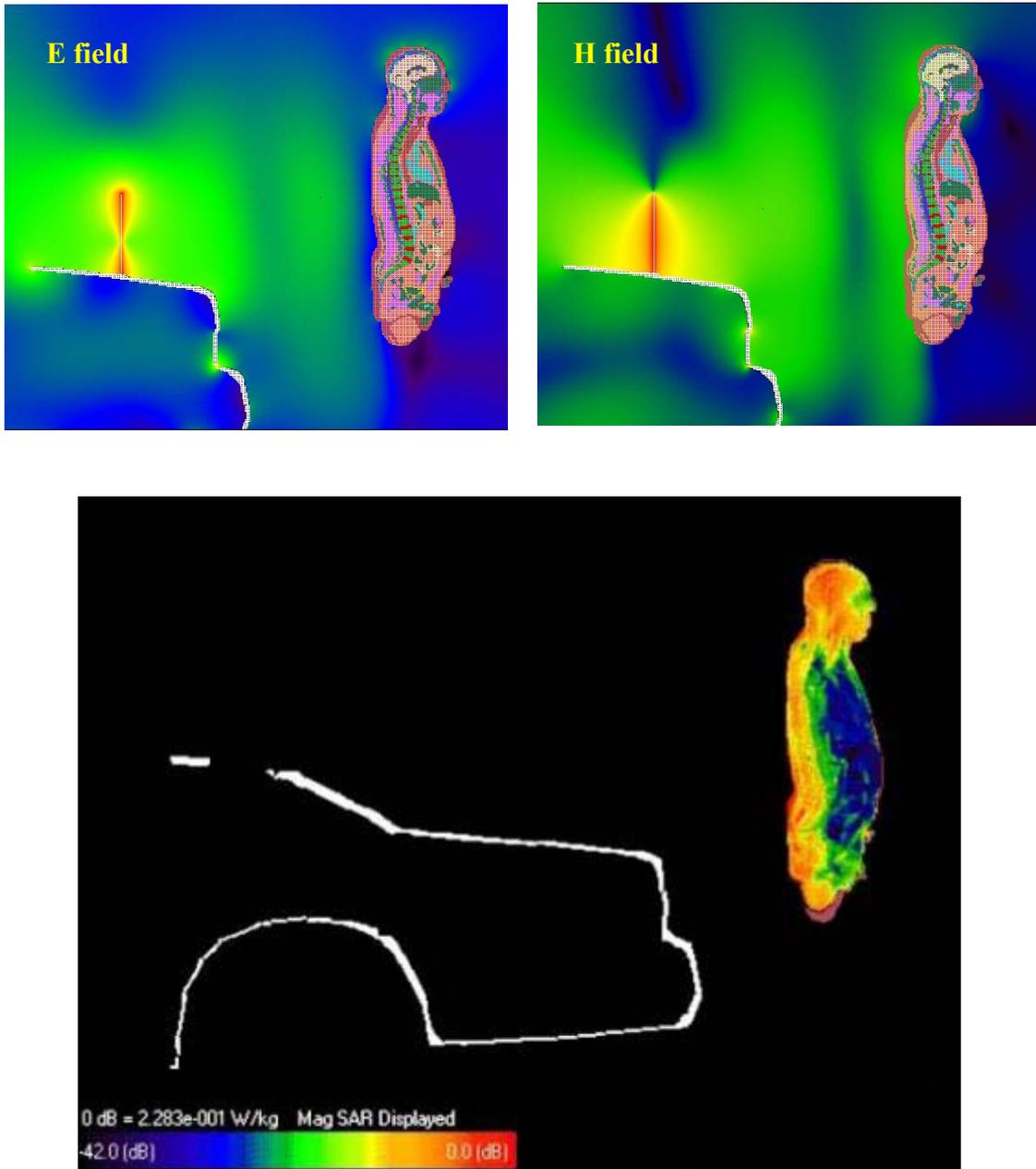
Figure 4. SAR and field distribution at 380 MHz for the bystander at 90 cm from the HAE6013A antenna, placed in the center of the trunk, when facing back to the car at 45 degrees. This is the condition with the overall maximum whole body average SAR for the bystander exposure. The field contour plots in the figure are relative to the middle cut plane of the bystander.
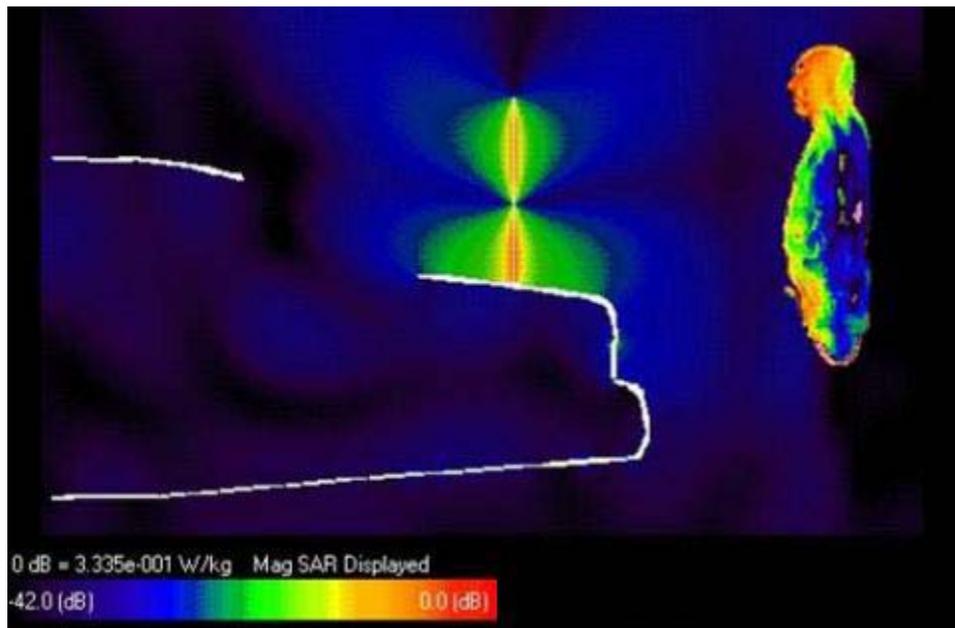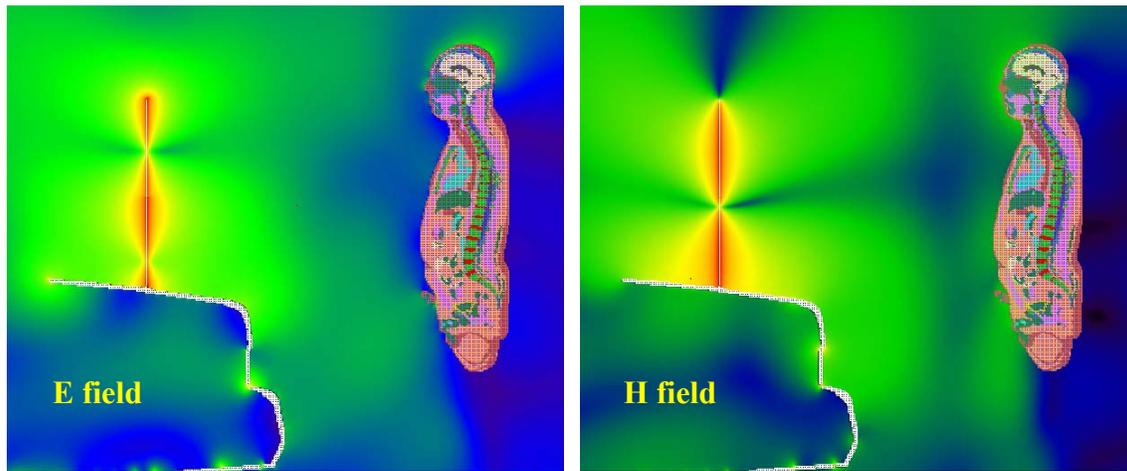
Figure 5. SAR and field distribution at 380 MHz for the bystander at 90 cm from the HAE6010A antenna, placed in the center of the trunk, when facing the car at 0 degrees.
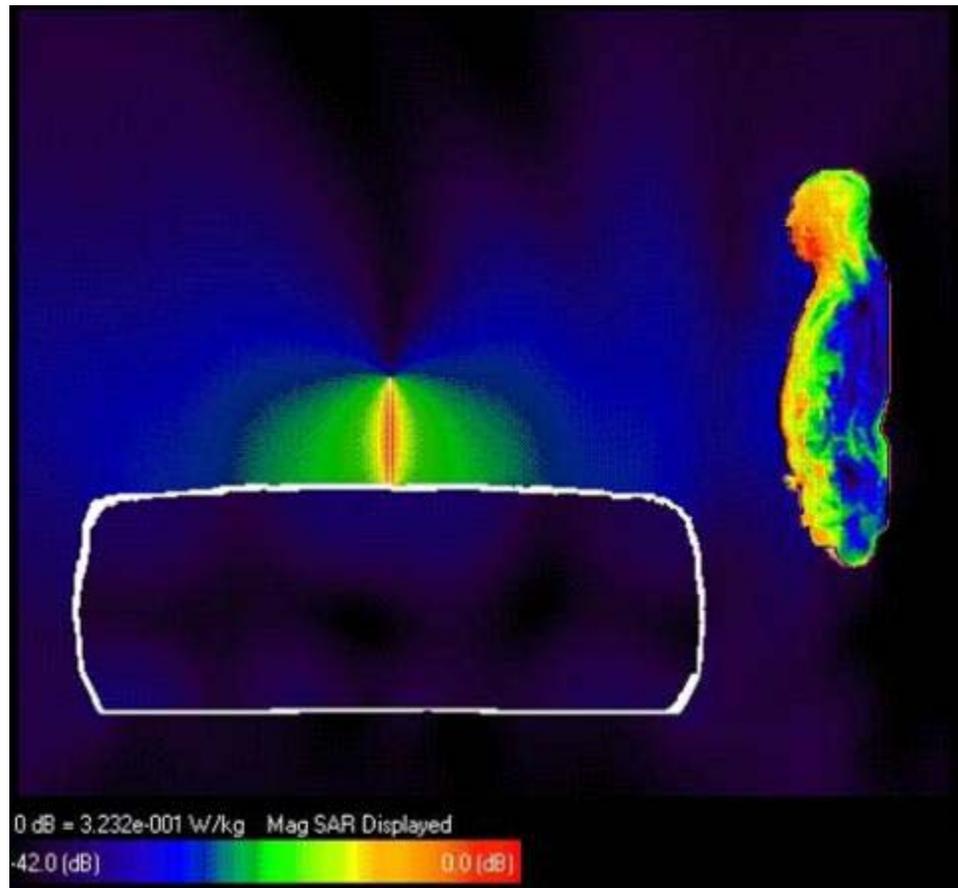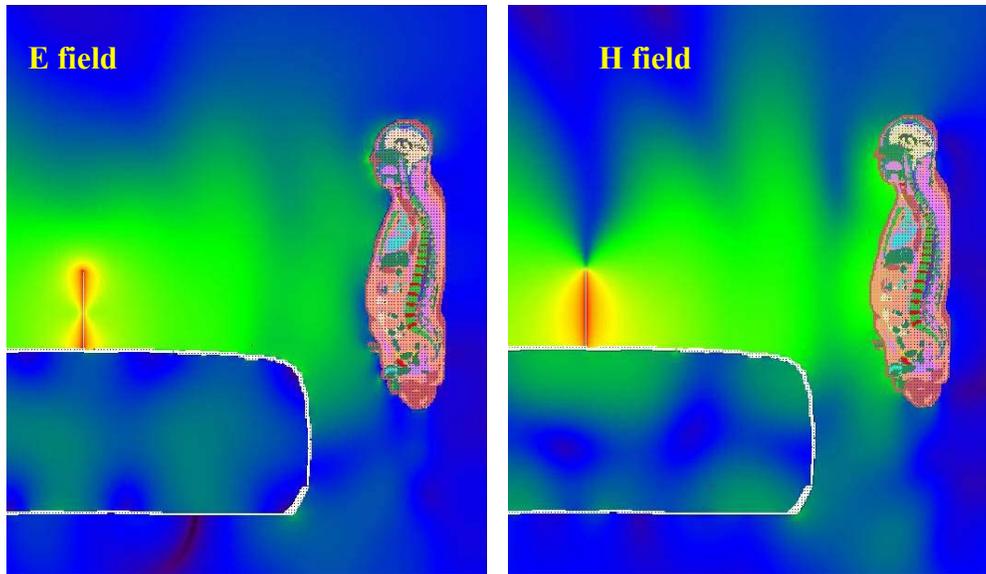
Figure 6. SAR and field distribution at 425 MHz for the bystander at 90 cm from the HAE6013A antenna, placed in the center of the trunk, when facing the car at 90 degrees.

Results of SAR computations for car passengers

The 14 test conditions requiring SAR computations are summarized in Table III, together with the antenna data and the SAR results. The conditions are for antenna mounted on the trunk. The passenger is located in the center or on the side of the rear seat. The passenger model is surrounded by air, as the seat, which is made out of poorly conductive fabrics, is not included in the computational model. All the transmit frequency, antenna length, and passenger location combinations reported in Table II have been simulated individually. The maximum peak 1-g SAR is 0.9 W/kg, while the maximum whole-body average SAR is 0.032 W/kg.

Table II: Results of the SAR computations for passenger exposure (50% talk-time).

MPE Table #	Mount location	Antenna Kit #	Antenna length		Freq [MHz]	Exposure location	SAR [W/kg]	
			Physical	XFDTD			1-g	WB
28	Trunk	**HAE4011A**	72.7 cm	72.5 cm	460	center	0.28	0.010
46	Trunk	**HAE4011A**	72.7 cm	72.5 cm	450	center	0.43	0.014
32	Trunk	**HAE6010A**	63.5 cm	63.5 cm	425	center	0.42	0.020
54	Trunk	**HAE6010A**	63.5 cm	63.5 cm	380	center	0.41	0.021
30	Trunk	**HAE6013A**	29 cm	29 cm	425	center	0.52	0.022
50	Trunk	**HAE6013A**	29 cm	29 cm	380	center	0.53	0.026
52	Trunk	**HAE6013A**	29 cm	29 cm	470	center	0.51	0.018
28	Trunk	**HAE4011A**	72.7 cm	72.5 cm	460	side	0.45	0.009
46	Trunk	**HAE4011A**	72.7 cm	72.5 cm	450	side	0.50	0.013
32	Trunk	**HAE6010A**	63.5 cm	63.5 cm	425	side	0.51	0.021
54	Trunk	**HAE6010A**	63.5 cm	63.5 cm	380	side	0.55	0.022
30	Trunk	**HAE6013A**	29 cm	29 cm	425	side	0.62	0.028
50	Trunk	**HAE6013A**	29 cm	29 cm	380	side	0.90	0.032
52	Trunk	**HAE6013A**	29 cm	29 cm	470	side	0.71	0.025

The SAR distribution in the passenger model in the exposure condition that gave highest 1-g SAR is reported in Fig. 7 (380 MHz, passenger in the side of the back seat, HAE6013A antenna). The same condition produced highest whole body average SAR.
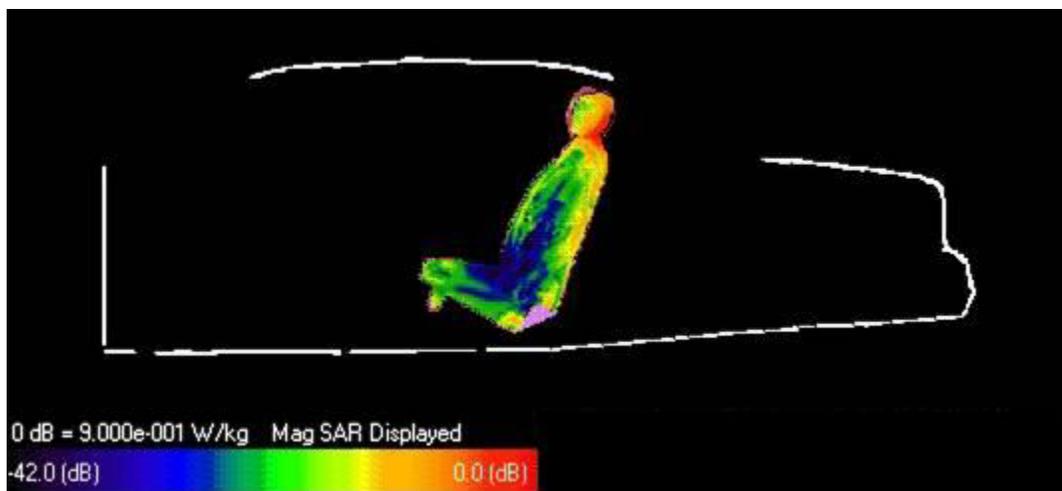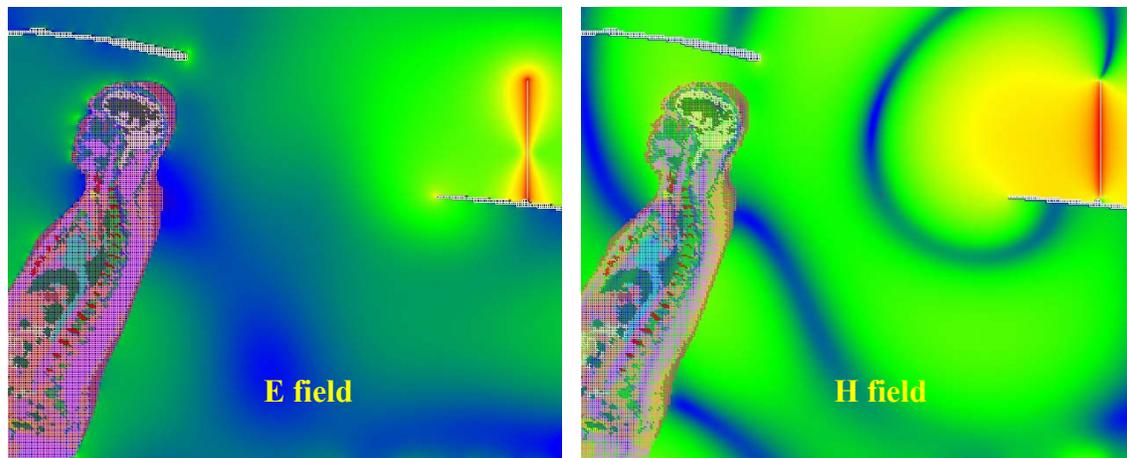
Figure 7. SAR and field distribution at 380 MHz in the passenger located in the side of the back seat, produced by the trunk-mount HAE6013A antenna. The contour plot in the figure is relative to the plane where the peak 1-g average SAR for this exposure condition occurs.

The SAR distributions for the passenger in the center of the back seat for different types of simulated antennas (HAE6013A, HAE6010A and HAE4011A) are shown in Fig. 8, Fig. 9 and Fig. 10. Fig. 9 and Fig. 10 also show the H field amplitude distribution relative to the plane where antenna is located.
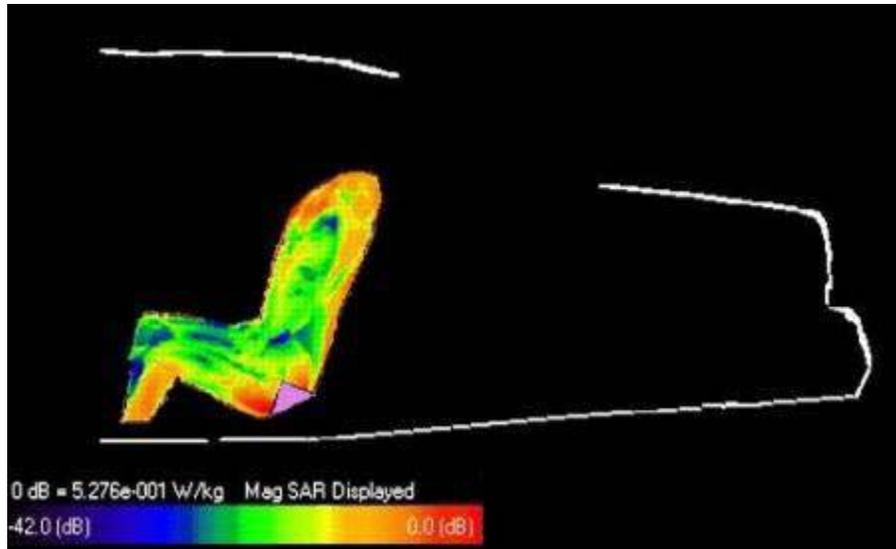
Figure 8. SAR distribution at 380 MHz in the passenger located in the center of the back seat, produced by the trunk-mount HAE6013A antenna. The contour plot in the figure is relative to the plane where the peak 1-g average SAR for this exposure condition occurs.
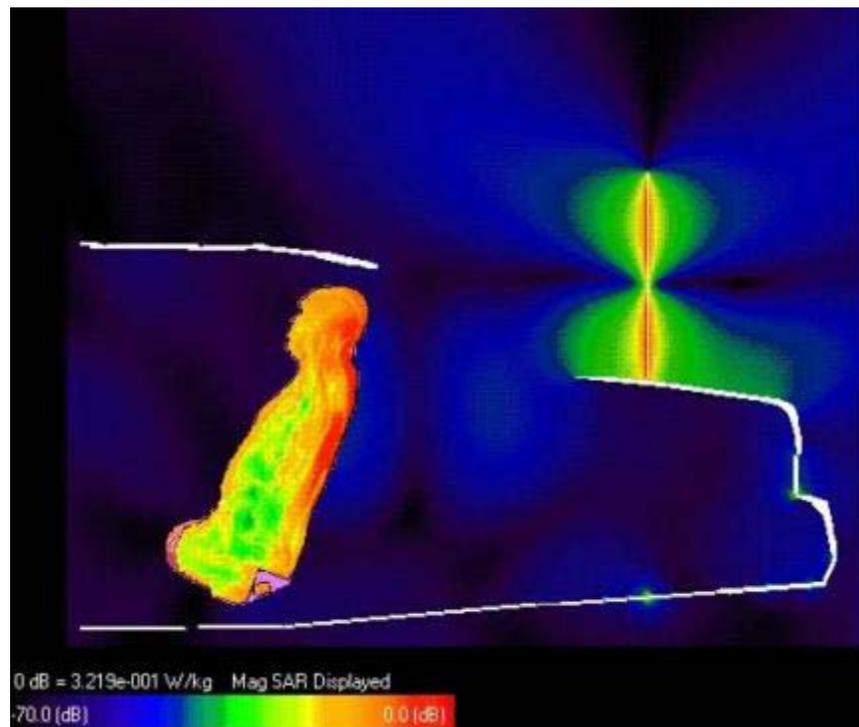

Figure 9. SAR and H field distribution at 380 MHz in the passenger located in the center of the back seat, produced by the trunk-mount HAE6010A antenna.
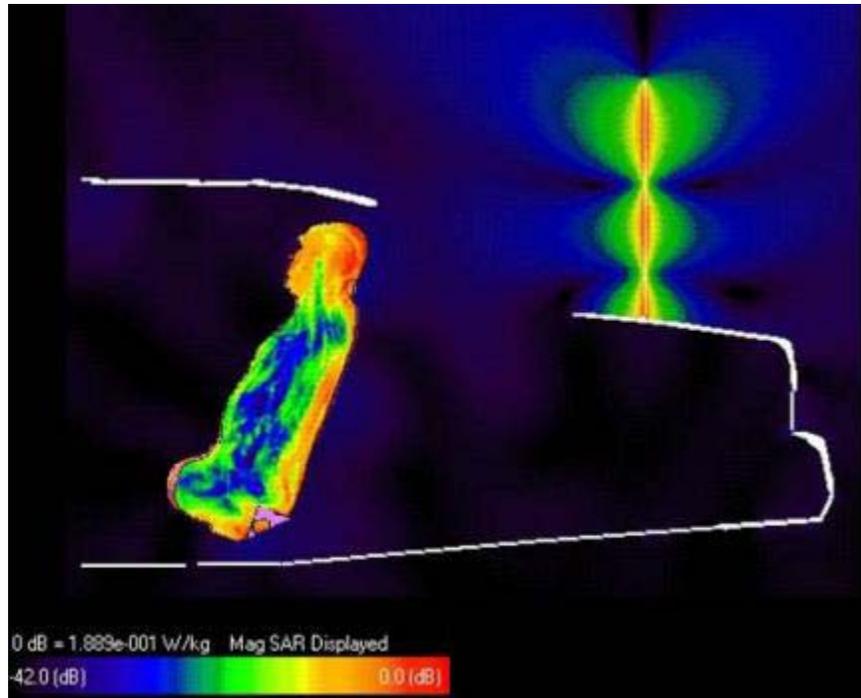
Figure 10. SAR and H field distribution at 450 MHz in the passenger located in the center of the back seat, produced by the trunk-mount HAE4011A antenna.

Conclusions

Under the test conditions described for evaluating passenger and bystander exposure to the RF electromagnetic fields emitted by vehicle-mounted antennas used in conjunction with this mobile radio product, the present analysis shows that the computed SAR values are compliant with the FCC exposure limits for the general public.

References

[1] IEEE Standard C95.1-1999. *IEEE Standard for Safety Levels with Respect to Human Exposure to RF Electromagnetic Fields*, 3 kHz to 300 GHz.

[2] http://www.nlm.nih.gov/research/visible/visible_human.html

APPENDIX: SPECIFIC INFORMATION FOR SAR COMPUTATIONS

This appendix follows the structure outlined in Appendix B.III of the Supplement C to the FCC OET Bulletin 65. Most of the information regarding the code employed to perform the numerical computations has been adapted from the XFDTD™ v5.3 User Manual. Remcom Inc., owner of XFDTD™, is kindly acknowledged for the help provided.

1) Computational resources

a) A four-processor server (Mod. PowerEdge 6650, by Dell Computers Inc.) equipped with four 1.4 GHz Xeon microprocessors and 4 GB D-RAM (3 GB available for running applications) was employed for all simulations.

b) The memory requirement was between 2 GB and 3 GB in all cases. Using the above-mentioned server with all four processors operating concurrently, the typical simulation would run for 22 hours.

**2) FDTD algorithm implementation and validation**

a) We employed a commercial code (XFDTD™ v5.3, by Remcom Inc.) that implements the classical Yee's FDTD formulation [1]. The solution domain was discretized according to a rectangular grid with a uniform 5 mm step in all directions. Sub-gridding was not used. Liao's absorbing boundary conditions [2] are set at the domain boundary to simulate free space radiation processes. The excitation is a lumped voltage generator with 50-ohm source impedance. The code allows selecting *wire objects* without specifying their radius. We used a wire to represent the antenna. The car body is modeled by solid metal. We did not employ the "thin wire" algorithm in XFDTD™ since the antenna radius was never smaller than one-fifth the voxel dimension. In fact, the XFDTD™ manual specifies that

"Thin Wire materials may be used in special situations where a wire with a radius much smaller than the cell size is required… in cases where the wire radius is important to the calculation and is less than approximately 1/5 the cell size, the thin wire material may be used to accurately simulate the correct wire dimensions."

The voxel size in all our simulations was 5 mm, and the antenna radius is always at least 1 mm (1 mm for the short quarter-wave antennas and 1.5 mm for the long gain antennas), so there was no need to specify a "thin wire" material. Pictures of the HAE6013A, HAE6010A and HAE4011A antennas are presented below.

The X-ray of the reactive load in the center of the HAE4011A and HAE6010A antennas are also presented in the next picture below. Those elements are significantly shorter than the length of the antenna and are about 1/40 of the wavelength at center operating frequency. They were modeled in XFDTD as lumped reactive elements.
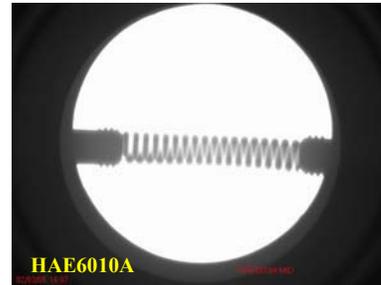

b) XFDTD™ is one of the most widely employed commercial codes for electromagnetic simulations. It has gone through extensive validation and has proven its accuracy over time in many different applications. One example is provided in [3].

We carried out a validation of the code algorithm by running the canonical test case involving a half-wave wire dipole. The dipole is 0.47 times the free space wavelength at 421.5 MHz, i.e., 33.5 cm long. The discretization used in the model was uniform in all directions and equal to 5 mm, so the dipole was 67 cells long. Also in this case, the "thin wire" model was not needed. The following picture shows XFDTD™ outputs regarding the antenna feed-point impedance (74.3 + j 2.0 ohm), as well as qualitative distributions of the total E and H fields near the dipole. The radiation pattern is shown as well (one lobe in elevation). As expected, the 3 dB beam width is about 78 degrees.
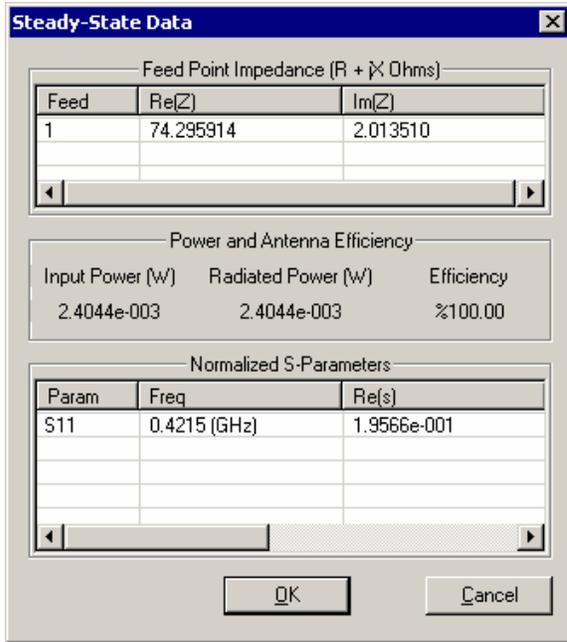
Total E-field **Total H-field**

dBi

3 dB

~78⁰

Elevation Angle [degrees]
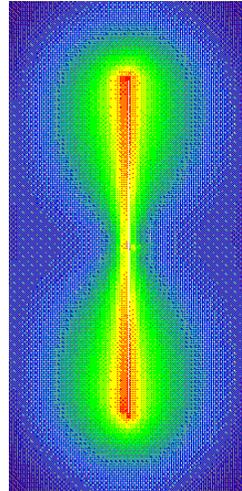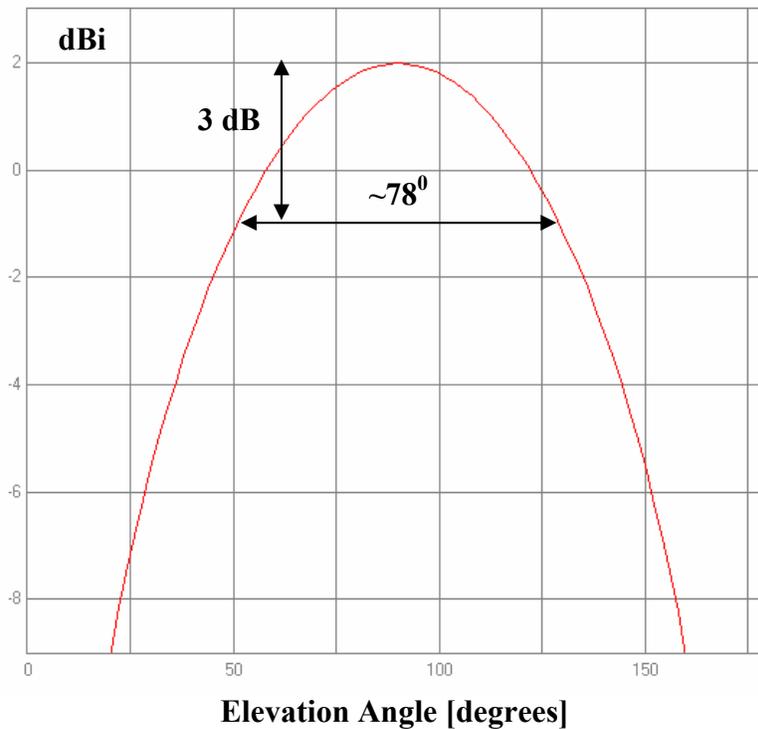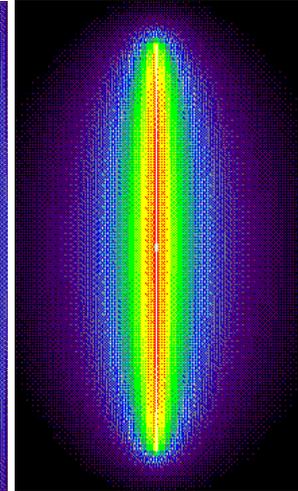
We also compared the XFDTD™ result with the results derived from NEC [4], which is a code based on the method of moments. In this case, we used a dipole with radius 1 mm, length 33.5 cm, and the discretization is 5 mm. The corresponding input impedance at 421.5 MHz is 71.7-j1.0 ohm. Its frequency dependence is reported in the following figure.
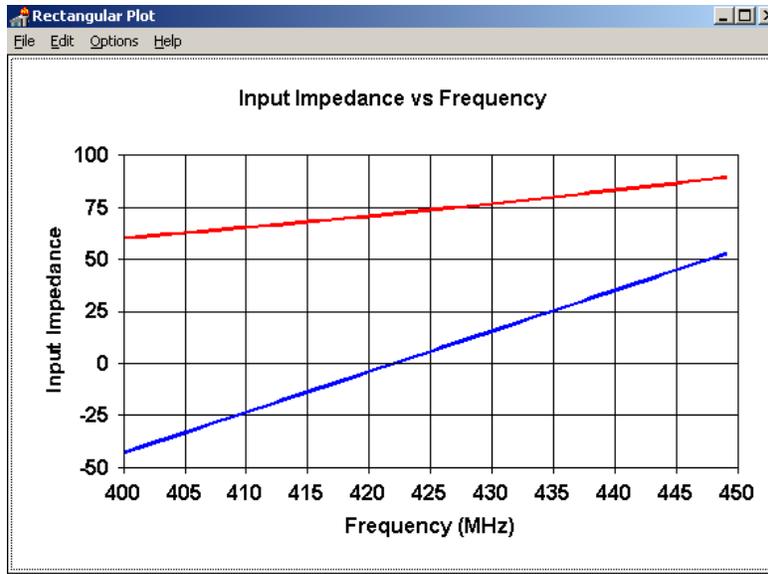
This validation ensures that the input impedance calculation is carried out correctly in XFDTD™, thereby enabling accurate estimates of the radiated power. It further ensures that the wire model employed in XFDTD™, which we used to model the antennas, produces physically meaningful current and fields distributions. Both these aspects ensure that the field quantities are correctly computed both in terms of absolute amplitude and relative distribution.

3) Computational parameters

a) The following table reports the main parameters of the FDTD model employed to perform our computational analysis:

| PARAMETER	X	Y	Z
Voxel size	5 mm	5 mm	5 mm
Maximum domain dimensions employed for bystander computations (in voxels), (for 0 degree and 45 degree bystander position)	407	476	430
Maximum domain dimensions employed for bystander computations (in voxels), (for 90 degree bystander position)	507	365	432
Maximum domain dimensions employed for passenger computations (in voxels)	400	489	419
Time step	Exactly equal to Courant limit (typically 10 *ps* at this frequency, with the body model)		
Objects separation from FDTD boundary (voxels)	>10	>10	>10
Number of time steps for passenger	At least 4000 in all simulations		
Number of time steps for bystander	4000 in all simulations		
Excitation	Sinusoidal (approx. 18 periods)		

b) In order to fit the model within a grid size that would not use up the available memory,

we chopped the hood of the car and the feet of the human model.

4) Phantom model implementation and validation

a) The FDTD mesh of a male human body was created using digitized data in the form of transverse color images. The data is from the *visible human project* sponsored by the National Library of Medicine (NLM) and is available via the Internet (http://www.nlm.nih.gov/research/visible/visible_human.html). The male data set consists of MRI, CT and anatomical images. Axial MRI images of the head and neck and longitudinal sections of the rest of the body are available at 4 mm intervals. The MRI images have 256 pixel by 256 pixel resolution. Each pixel has 12 bits of gray tone resolution. The CT data consists of axial CT scans of the entire body taken at 1 mm intervals at a resolution of 512 pixels by 512 pixels where each pixel is made up of 12 bits of gray tone. The axial anatomical images are 2048 pixels by 1216 pixels where each pixel is defined by 24 bits of color. The anatomical cross sections are also at 1 mm intervals and coincide with the CT axial images. There are 1871 cross sections. The XFDTD™ High Fidelity Body Mesh uses 5x5x5 mm cells and has dimensions 136 x 87 x 397. Dr. Michael Smith and Dr. Chris Collins of the Milton S. Hershey Medical Center, Hershey, Pa, created the High Fidelity Body mesh. Details of body model creation are given in the *methods* section in [5]. The body mesh contains 23 tissues materials. Measured values for the tissue parameters for a broad frequency range are included with the mesh data. The correct values are interpolated from the table of measured data and entered into the appropriate mesh variables. The tissue conductivity and permittivity variation *vs.* frequency is included in the XFDTD™ calculation by a multiple-pole approximation to the Cole-Cole approximated tissue parameters reported by Camelia Gabriel, Ph.D., and Sami Gabriel, M. Sc. (http://www.brooks.af.mil/AFRL/HED/hedr/reports/dielectric/home.html).

In order to fit the car and bystander model within the volume allowed by the available RAM, the feet of the XFDTD™ High Fidelity Body Mesh were cut away, thereby reducing the model length by about 16 cm (32 voxels). Notice that the original model's feet are not flat and parallel to ground as if he were standing, but are inclined downwards. Therefore, we estimated that the actual reduction in body length is 9 cm. The following figure shows the cross section of the model used in the bystander computations, compared with the original XFDTD™ High Fidelity Body Mesh.
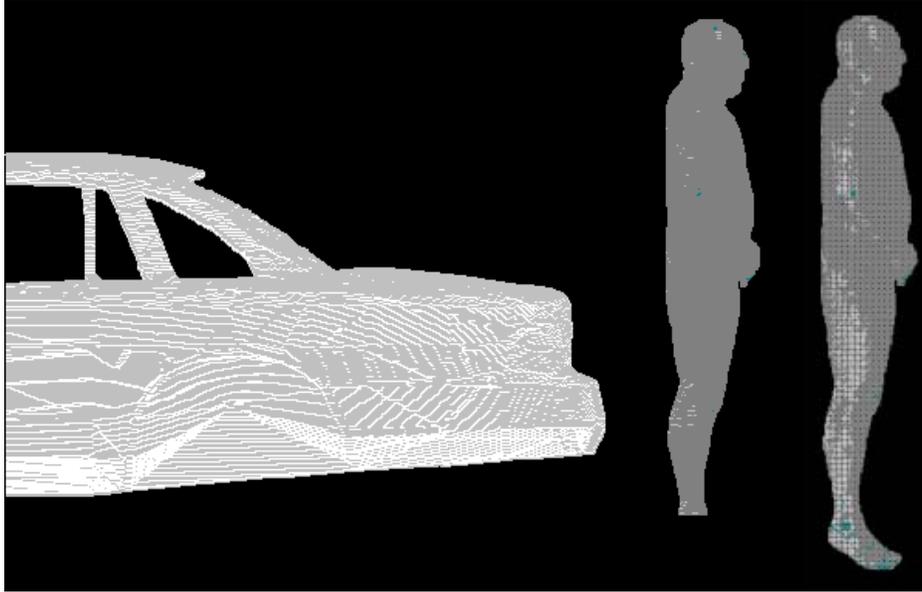
b) The XFDTD™ High Fidelity Body Mesh model correctly represents the anatomical structure and the dielectric properties of body tissues, so it is appropriate for determining the highest exposure expected for normal device operation. The model is a standing subject. By taking advantage of the XFDTD built-in ability to segment and rotate bodies, the full body model was cut at the hip and the knees, then the various body parts were translated and rotated in order to arrange them in a way so as to represent a passenger model. The passenger model was then defined as a single XFDTD element that could be inserted in the car model at different location in the back seat

c) One example of the accuracy of XFDTD™ for computing SAR has been provided in [6]. The study reported in [6] is relative to a large-scale benchmark of measurement and computational tools carried out within the IEEE Standards Coordinating Committee 34, Sub-Committee 2.

5) Tissue dielectric parameters

a) The following table reports the dielectric properties used by XFDTD™ for the 23 body tissue materials in the High Fidelity Body Mesh at 450 MHz (mid-band for this VHF mobile radio product).

#	Tissue	ε_r	σ (S/m)	Density (kg/m^3)
1	skin	41.5	0.57	1125
2	tendon, pancreas, prostate, aorta, liver, other	50.3	0.76	1151
3	fat, yellow marrow	5.02	0.05	943
4	cortical bone	13.4	0.11	1850
5	cancellous bone	21.0	0.23	1080
6	blood	57.2	1.72	1057

| 7	muscle, heart, spleen, colon, tongue	63.5	0.99	1059
8	gray matter, cerebellum	54.1	0.88	1035.5
9	white matter	39.7	0.54	1027.4
10	CSF	68.9	2.32	1000
11	sclera/cornea	54.4	1.04	1151
12	vitreous humor	68.3	1.56	1000
13	bladder	17.6	0.31	1132
14	nerve	35.5	0.50	1112
15	cartilage	43.4	0.66	1171
16	gall bladder bile	76.5	1.62	928
17	thyroid	59.8	0.82	1035.5
18	stomach/esophagus	74.4	1.13	1126
19	lung	52.8	0.72	563
20	kidney	57.0	1.16	1147
21	testis	65.2	1.13	1158
22	lens	51.9	0.71	1163
23	small intestine	73.7	2.07	1153

b) The tissue types and dielectric parameters used in the SAR computation are appropriate for determining the highest exposure expected for normal device operation, because they are derived from measurements performed on real biological tissues (http://www.brooks.af.mil/AFRL/HED/hedr/reports/dielectric/home.html).

c) The tabulated list of the dielectric parameters used in phantom models is provided at point 5(a). As regards the device (car plus antenna), we used perfect electric conductors.

6) Transmitter model implementation and validation

a) The essential features that must be modeled correctly for the particular test device model to be valid are:

- Car body. We developed one very similar to the car used for MPE measurements, so as to be able to correlate measured and simulated field values. The model was imported in XFDTD™ from a CAD model that is commercially available at http://www.3dcadbrowser.com/
- Antenna. We used a straight wire in all cases, even though the gain antenna has a base coil for tuning. All the coil does is compensating for excess capacitance due to the antenna being slightly longer than half a wavelength. We do not need to do that in the model, as we used normalization with respect to the net radiated power, which is determined by the input resistance only. In this way, we neglect mismatch losses and artificially produce an overestimation of the SAR, thereby introducing a conservative bias in the model.
- Antenna location. We used the same location, relative to the edge of the car trunk, the backseat, or the roof, used in the MPE measurements. The following pictures show a lateral and a perspective view of the whole model (XFDTD™ does not show wires in this type of view, that is why the antenna is not visible).
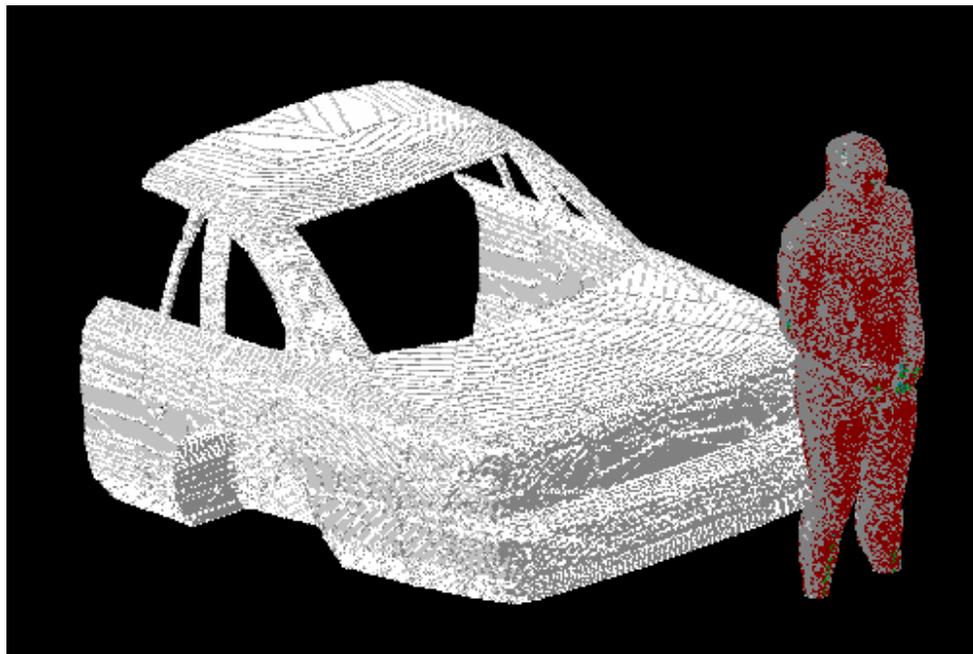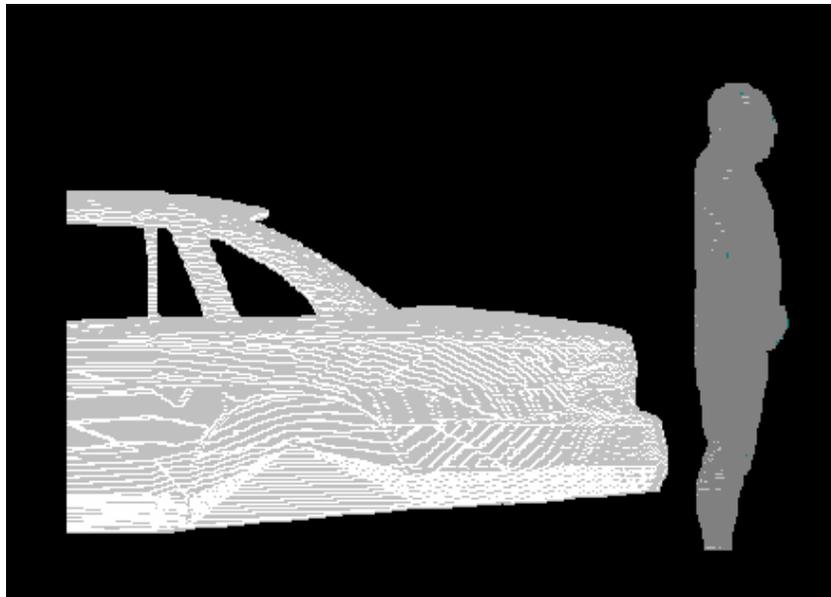
The car model is constituted by perfect electric conductor and does not include wheels in order to reduce its complexity. The passenger model is surrounded by air, as the seat, which is made out of poorly conductive fabrics, is not included in the computational model. The pavement has not been included in the model.

The passenger and bystander models were validated for similar antenna and frequency conditions by comparing the MPE measurements at two UHF frequencies (421.5 MHz and 425 MHz). The validation at 421.5 MHz was performed in 2004 (FCC ID#ABZ99FT4064). The corresponding MPE measurements are reported in the compliance report relative to FCC ID#ABZ99FT4064. The comparison results are

presented below, according to following definitions for the equivalent power densities (based on E or H-field):

$$S_E = \frac{|\mathbf{E}|^2}{2\eta}, \quad S_H = \frac{\eta}{2}|\mathbf{H}|^2, \quad \eta = 377 \, \Omega$$

<u>Passenger with 17.5 cm monopole antenna (HAE4002A 421.5 MHz)</u>

The following figure of the test model shows the car model, where the yellow dots individuate the back seat, as it can be observed from the other figure showing the cross section of the passenger. The comparison has been performed by taking the average of the computed steady-state field values at the six dotted locations, corresponding to the head, chest, and legs along the yellow dots line, and comparing them with the average of the MPE measurements performed at the head, chest and legs locations. Such a comparison is carried out at the same rms power level (22 W, including the 50% duty factor) used in the MPE measurements.
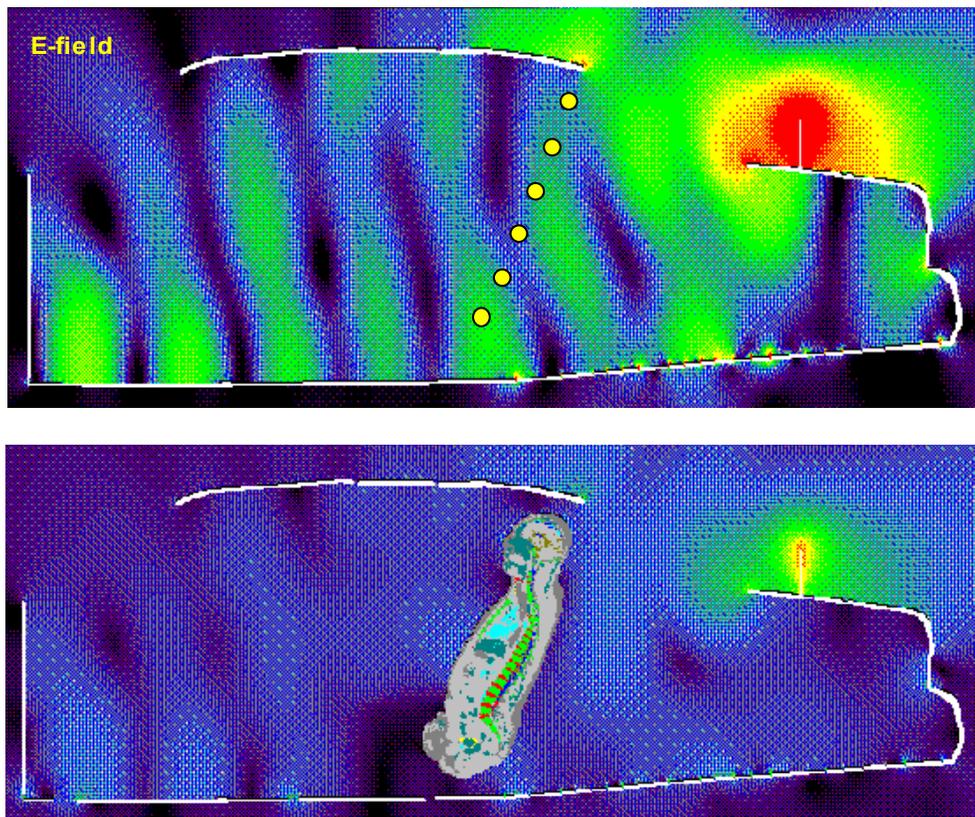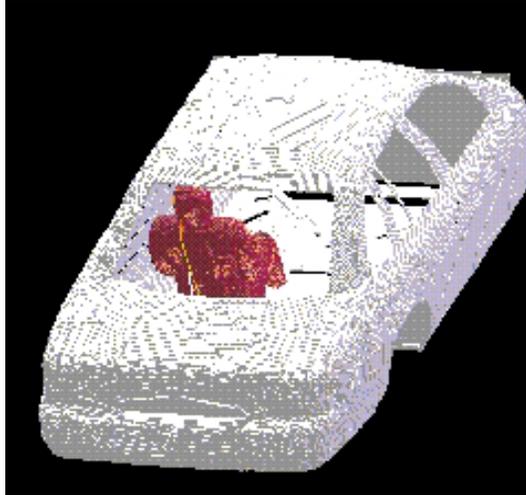
The equivalent power density (S) is computed from the E-field and the H-field separately. The following table reports the E-field values computed by XFDTD™ at the six locations, and the corresponding power density.

Location Number	E-field, V/m	Eq. Power Density 1.0 V source	Scaled Power Dens. 22 W output, mW/cm^2
1	5.83E-01	4.51E-04	4.41E-01
2	6.31E-01	5.28E-04	5.16E-01
3	6.50E-01	5.60E-04	5.48E-01
4	5.50E-01	4.01E-04	3.92E-01
5	4.50E-01	2.69E-04	2.63E-01
6	7.80E-01	8.07E-04	7.89E-01
Equivalent average Power Density			**4.92E-01**

Location Number	B-field, Weber/m2	Eq. Power Density 1.0 V source	Scaled Power Dens. 22 W output, mW/cm^2
1	2.26E-09	0.00061	5.96E-01
2	9.00E-10	0.00010	9.45E-02
3	1.20E-09	0.00017	1.68E-01
4	2.20E-09	0.00058	5.65E-01
5	1.90E-09	0.00043	4.21E-01
6	9.00E-10	0.00010	9.45E-02
Equivalent average Power Density			**3.23E-01**

The input impedance is 36.2+j24.8 ohm, therefore the radiated power (considering the mismatch to the 50 ohm unitary voltage source) is 2.25E-3 W, therefore a factor equal to 9779 is required to scale up to 22 W radiated. The corresponding scaled-up power

22

densities are reported in the tables above, which show that the simulation overestimates the average power density from the MPE measurements (0.29 mW/cm^2), as derived from the measured E-field reported in the following table:

Position	SE (meas), 22 W output mW/cm^2
Head	0.38
Chest	0.33
Lower Trunk	0.16

The simulations tend to overestimate the average power density levels, which is understandable since there are no ohmic losses and perfect impedance matching is enforced in the computational models. Based on these results, we conclude that the simulation will produce slight exposure overestimates (about12%).

b) Descriptions and illustrations showing the correspondence between the modeled test device and the actual device, with respect to shape, size, dimensions and near-field radiating characteristics, are found in the main report.

c) Verification that the test device model is equivalent to the actual device for predicting the SAR distributions descends from the fact that the car and antenna size and location in the numerical model correspond to those used in the measurements.

d) The peak SAR is in the neck region for the passenger, which is in line with MPE measurements and predictions.

Passenger with 63.5 cm monopole antenna (HAE6010A 425 MHz)

The following figures show the car model with the field distribution in the horizontal planes where the MPE measurements have been performed. The comparison has been performed by taking the average of the computed steady-state field values at the three locations, corresponding to the head, chest, and lower trunk, and comparing them with the average of the MPE measurements performed at the head, chest and lower trunk locations. Such a comparison is carried out at the same rms power level (61.5 W, including the 50% duty factor) used in the MPE measurements.
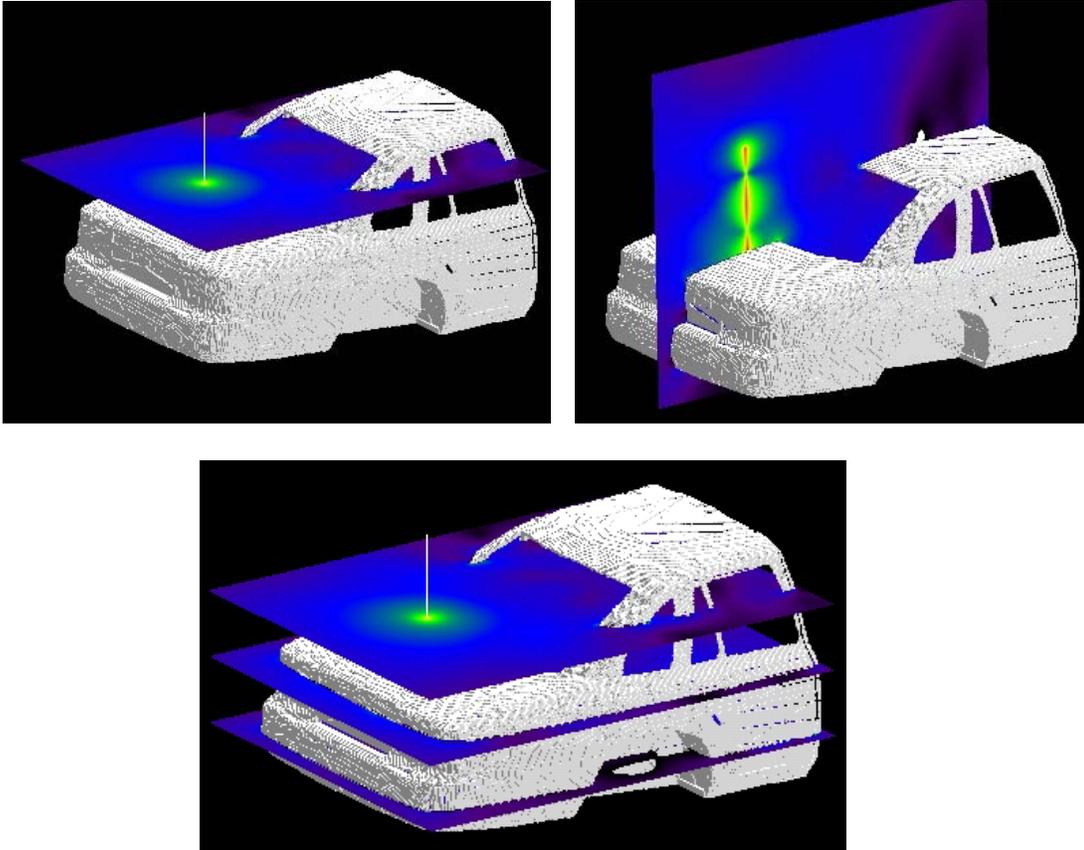
The equivalent power density (S) is computed from the E-field. The following table reports the E-field values computed by XFDTD™ at the three locations, and the corresponding power density.

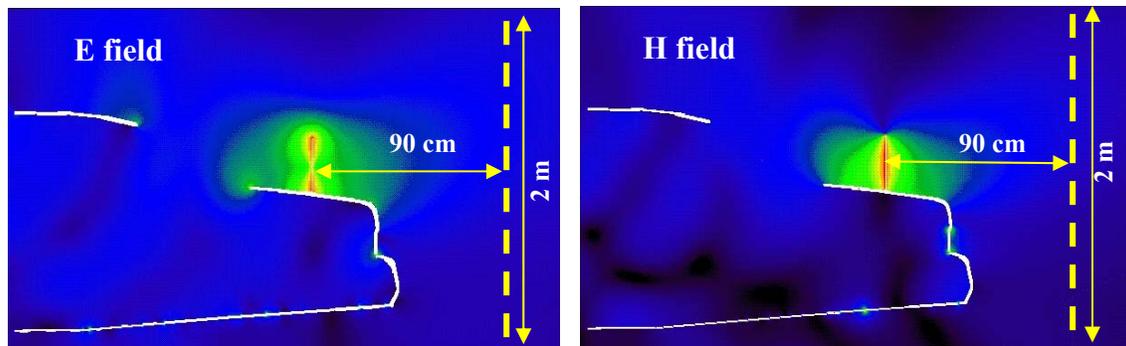| Location Number	E-field, V/m	Eq. Power Density 1.0 V source	Scaled Power Dens. 61.5 W output, mW/cm^2
1	2.10E-01	5.85E-05	0.561
2	3.66E-01	1.78E-04	1.70
3	1.72E-01	3.92E-04	0.376
Equivalent average Power Density			**0.88**

The corresponding scaled-up power densities are reported in the tables above, which show that the simulation overestimates the average power density from the MPE measurements (0.52 mW/cm^2), as derived from the measured E-field reported in the following table:
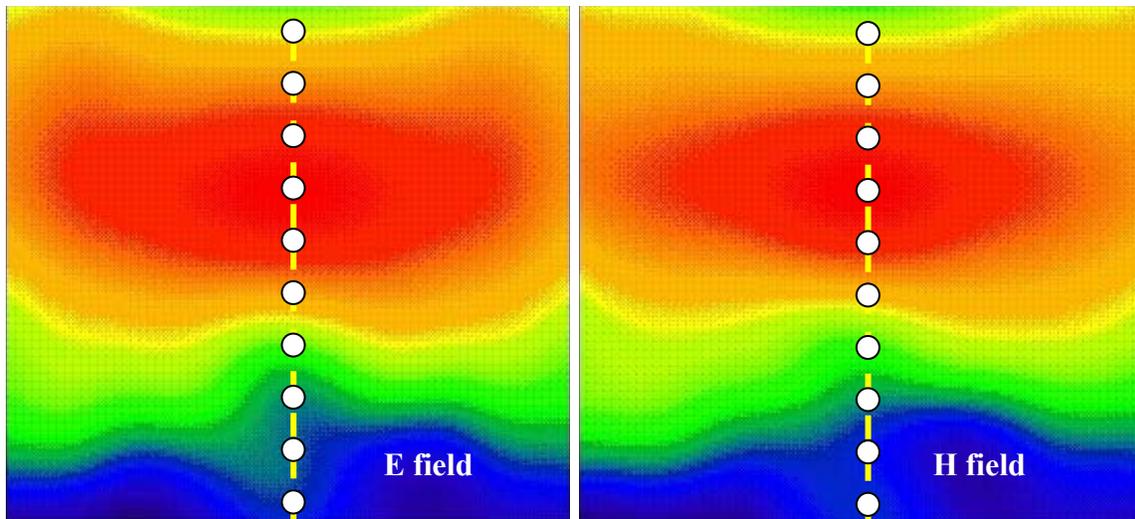
Position	SE (meas), 60 W output mW/cm^2
Head	0.72
Chest	0.64
Lower Trunk	0.19

The simulations tend to overestimate the average power density levels, which is understandable since there are no ohmic losses and perfect impedance matching is enforced in the computational models. Based on these results, we conclude that the simulation will produce exposure overestimates (about 69%).

Bystander with 29 cm monopole antenna (HAE6013A 425 MHz)

The following figures show the E-field and H-field distributions across a vertical plane passing for the antenna and cutting the car in half. As done in the measurements, the MPE is computed from both E-field and H-field distributions, along the yellow dotted line at 10 points spaced 20 cm apart from each other up to 2 m in height. These lines and the field evaluation points are approximately indicated in the figures. The E-field and H-field distributions in the vertical plane placed at 90 cm from the antenna, behind the case, are shown as well. The points where the fields are sampled to determine the equivalent power density (S) are approximately indicated by the white dots. A picture of the antenna is not reported because it is identical to the HAE6013A.
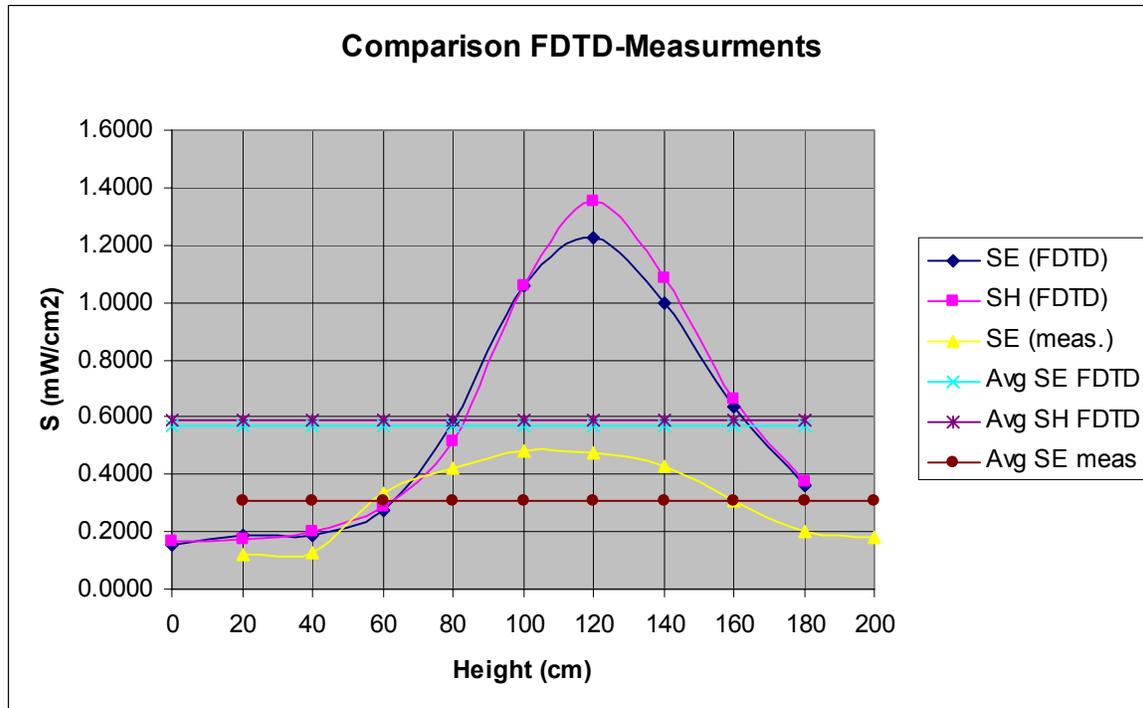
E field   H field

The following table reports the field values computed by XFDTD™ and the corresponding power density values. The average exposure levels are computed as well.
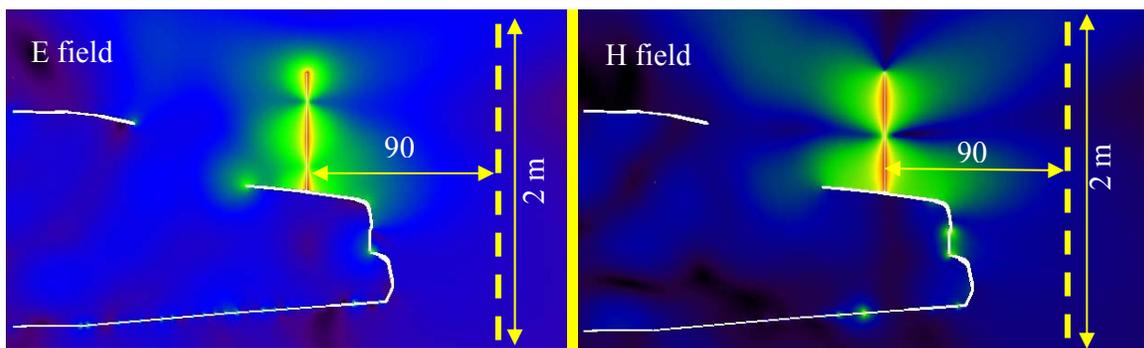
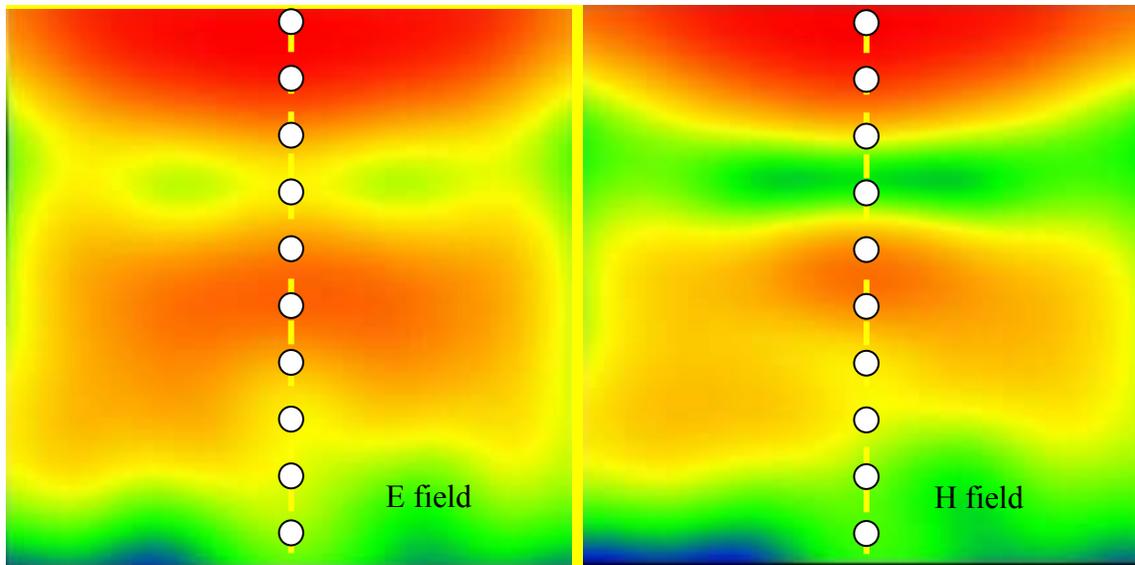| Height (cm)	E (V/m)	S_E (W/m^2)	H (A/m)	S_H (W/m^2)
0	1.05E-01	1.46E-05	2.90E-05	1.589E-05
20	1.14E-01	1.72E-05	2.90E-05	1.598E-05
40	1.16E-01	1.78E-05	3.14E-05	1.871E-05
60	1.39E-01	2.56E-05	3.75E-05	2.669E-05
80	2.03E-01	5.47E-05	5.03E-05	4.795E-05
100	2.73E-01	9.88E-05	7.23E-05	9.923E-05
120	2.94E-01	1.15E-04	8.17E-05	1.266E-04
140	2.65E-01	9.31E-05	7.32E-05	1.016E-04
160	2.12E-01	5.96E-05	5.73E-05	6.219E-05
180	1.60E-01	3.40E-05	4.32E-05	3.531E-05
Average S_E		5.302E-05	Average S_H	5.501E-05

Since the conducted power during the MPE measurement was 123 W the calculated power density was then scaled up for 61.5 W radiated power (taking into account 50% talk time). This model does not include the mismatch loss, loss in the cable and finite conductivity of the car surface and as represents a conservative model for exposure assessment. The scaled-up power density values for 61.5 W radiated power are 5.67 W/m^2 (E), and 5.88 W/m^2 (H), that correspond to 0.57 mW/cm^2 (E), and 0.59 mW/cm^2 (H). Measurements yielded average power density of 0.309 mW/cm^2 (E), which shows that the calculated power density is overestimated. The following graph shows a comparison between the measured power density and the simulated one, based on E or H fields, normalized to 61.5 W radiated power.

Comparison FDTD-Measurments

Bystander with 63.5 cm monopole antenna (HAE6010A 425 MHz)

The following figures show the E-field and H-field distributions across a vertical plane passing for the antenna and cutting the car in half. As done in the measurements, the MPE is computed from both E-field and H-field distributions, along the yellow dotted line at 10 points spaced 20 cm apart from each other up to 2 m in height. These lines and the field evaluation points are approximately indicated in the figures. The E-field and H-field distributions in the vertical plane placed at 90 cm from the antenna, behind the case, are shown as well. The points where the fields are sampled to determine the equivalent power density (S) are approximately indicated by the white dots. A picture of the antenna is not reported because it is identical to the HAE6010A.

E field   H field

The following table reports the field values computed by XFDTD™ and the corresponding power density values. The average exposure levels are computed as well.

Height (cm)	E (V/m)	S_E (W/m^2)	H (A/m)	S_H (W/m^2)
0	1.32E-01	2.31E-05	4.51E-10	2.43E-05
20	1.49E-01	2.94E-05	4.82E-10	2.77E-05
40	1.58E-01	3.31E-05	5.44E-10	3.53E-05
60	1.71E-01	3.88E-05	5.79E-10	4.00E-05
80	2.10E-01	5.85E-05	6.78E-10	5.48E-05
100	2.12E-01	5.96E-05	7.60E-10	6.89E-05
120	1.67E-01	3.70E-05	4.86E-10	2.82E-05
140	1.83E-01	4.44E-05	5.57E-10	3.70E-05
160	2.50E-01	8.29E-05	8.62E-10	8.86E-05
180	2.68E-01	9.53E-05	9.75E-10	1.13E-04
Average S_E		**5.38E-05**	**Average S_H**	**5.18E-05**

Since the conducted power during the MPE measurement was 123 W the calculated power density was then scaled up for 61.5 W radiated power (taking into account 50% talk time). This model does not include the mismatch loss, loss in the cable and finite conductivity of the car surface and as represents a conservative model for exposure assessment. The scaled-up power density values for 61.5 W radiated power are 5.25 W/m^2 (E), and 5.06 W/m^2 (H), that correspond to 0.52 mW/cm^2 (E), and 0.51 mW/cm^2 (H). Measurements yielded average power density of 0.204 mW/cm^2 (E), which shows that the calculated power density is overestimated. The following graph shows a comparison between the measured power density and the simulated one, based on E or H

fields, normalized to 61.5 W radiated power.

Comparison FDTD-Measurments
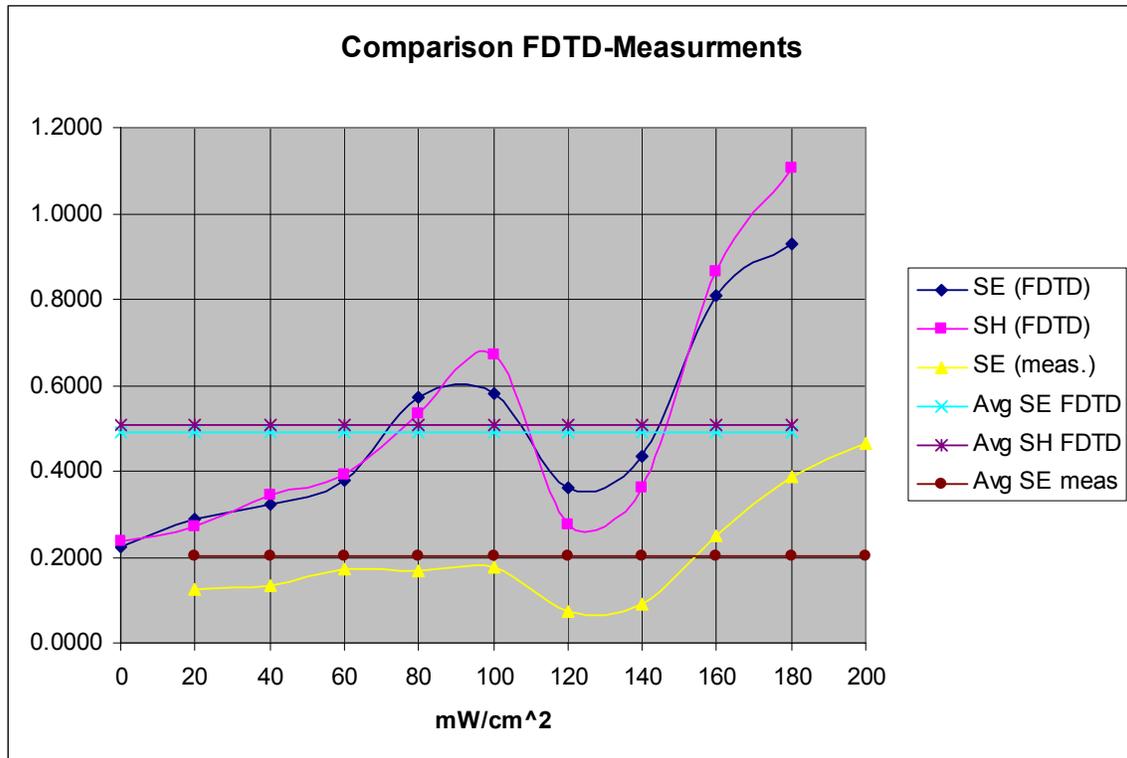
7) Test device positioning

a) A description of the device test positions used in the SAR computations is provided in the SAR report.

b) Illustrations showing the separation distances between the test device and the phantom for the tested configurations are provided in the SAR report.

8) Steady state termination procedures

a) The criteria used to determine that sinusoidal steady-state conditions have been reached throughout the computational domain for terminating the computations are based on the monitoring of field points to make sure they converge. For at least one passenger and one bystander exposure condition, we placed one "field sensor" near the antenna, others between the body and the domain boundary at different locations, and one inside the head of the model. In all simulations, isotropic E-field sensors were placed at opposite corners of the computational domain. We used isotropic E and H field "sensors", meaning that all three components of the fields are monitored at these points. The following figures show an example of the time waveforms at the field point sensors in the head and in two opposite points in the computational domain. In the latter case, we

selected points near the lowest and highest grid index points. They are shown together in the figure. The highest field levels are observed for the higher index point, as it is closer to the antenna. In all cases, the field reaches the steady-state after a few cycles.
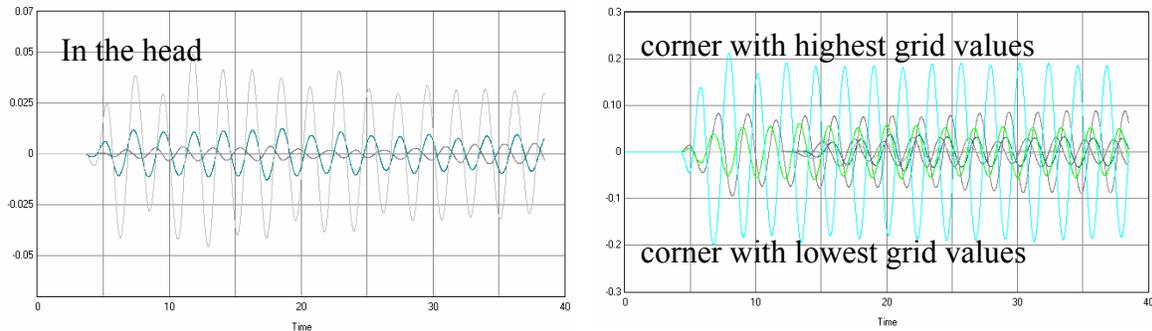
b) 4000 time steps were used, with a time step approximately equal to 10 *ps* (meeting the Courant criterion), which corresponds to 18 wave periods at 450 MHz.

c) The XFDTD™ algorithm determines the field phasors by using the so-called "two-equations two-unknowns" method. Details of the algorithm are explained in [7].

9) Computing peak SAR from field components

a) The twelve E-field phasors at the edges of each Yee voxel are combined to yield the SAR associated to that voxel. In particular, the average is performed on the SAR values computed at the 12 edges of each voxel. Notice that in XFDTD™ the dielectric tissue properties are assigned to the voxel edges, thereby allowing said averaging procedure.

b) The IEEE Standards Coordinating Committee 34, Sub-Committee 2 draft standard P1529 (June 2000) discusses several algorithms for volumetric SAR averaging. It states that "It is observed that while the 12 components algorithm is the most appropriate from the mathematical point of view, the differences in 1g SAR calculated with either the 12 or 6 component methods are negligible for practical mesh resolutions (below 5mm). On the other hand, it is shown that the 3 components approach may lead to significant errors." XFDTD™ employs the 12-component method, which is the one recommended in the draft standard, thus providing the best achievable accuracy.

10) One-gram averaged SAR procedures

a) XFDTD™ computes the Specific Absorption Rate (SAR) in each complete cell containing lossy dielectric material and with a non-zero material density. To be considered a complete cell, the twelve cell edges must belong to lossy dielectric materials. The averaging calculation uses an interpolation scheme for finding the averages. Cubical spaces centered on a cell are formed and the mass and average SAR of the sample cubes are found. The size of the sample cubes increases until the total mass of the enclosed exceeds either 1 or 10 grams. The mass and average SAR value of each

cube is saved and used to interpolate the average SAR values at either 1 or 10 grams. The interpolation is performed using two methods (polynomial fit and rational function fit) and the one with the lowest error is chosen. The sample cube must meet some conditions to be considered valid. The cube may contain some non-tissue cells, but some checks are performed on the distribution of the non-tissue cells. A valid cube will not contain an entire side or corner of non-tissue cells.

b) The sample cube increases in odd-numbered steps (1x1x1, 3x3x3, 5x5x5, etc) to remain centered on the desired cell. Since the visible human model employed herein has 5 mm resolution, the one-gram SAR is computed by averaging first over 1x1x1 voxels, corresponding to 0.125 cm^3 (not enough yet), and then over a 3x3x3 voxel cube, corresponding to about 3.4 cm^3, which is enough to include 1-g, and finally over a 5x5x5 voxel cube, corresponding to about 15.6 cm^3, which includes 10-g. The 1-g average SAR is computed by interpolating these three data points. This procedure is repeated in the surroundings of each voxel that is constituted by lossy materials, so as to determine the 1-g and/or 10-g SAR distributions.

c) As mentioned at points 10(a) and 10(b), the 1- gram average SAR is determined by interpolating the average SAR for the 1x1x1 , 3x3x3, and the 5x5x5 data points, corresponding to 0.125 cm^3, 3.4 cm^3, and 15.6 cm^3, respectively. Because the interpolation is carried out across three data points, the error introduced should be negligible because the interpolating curve crosses exactly the data points.

11) Total computational uncertainty – We derived an estimate for the uncertainty of FDTD methods in evaluating SAR by referring to [6]. In Fig. 7 in [6] it is shown that the deviation between SAR estimates using the XFDTD™ code and those measured with a compliance system are typically within 10% when the probe is away from the phantom surface so that boundary effects are negligible. In that example, the simulated SAR always exceeds the measured SAR.

As discussed in 6(a), a conservative bias has been introduced in the model so as to reduce concerns regarding the computational uncertainty related to the car modeling, antenna modeling, and phantom modeling. The results of the comparison between measurements and simulations presented in 6(a) suggest that the present model produces an overestimate of the exposure up to 80%. Such a conservative bias should eliminate the need for including uncertainty considerations in the SAR assessment.

12) Test results for determining SAR compliance

a) Illustrations showing the SAR distribution of dominant peak locations produced by the test transmitter, with respect to the phantom and test device, are provided in the SAR report.

b) The input impedance and the total power radiated under the impedance match conditions that occur at the test frequency are provided by XFDTD™. XFDTD™ computes the input impedance by following the method outlined in [8], which consists in

performing the integration of the steady-state magnetic field around the feed point edge to compute the steady-state feed point current (I), which is then used to divide the feed-gap steady-state voltage (V). The net *rms* radiated power is computed as

$$P_{XFDTD} = \frac{1}{2}\text{Re}\{VI^*\}$$

Both the input impedance and the net rms radiated power are provided by XFDTD™ at the end of each individual simulation.

We normalize the SAR to such a power, thereby obtaining SAR per radiated Watt (*normalized SAR*) values for the whole body and the 1-g SAR. Finally, we multiply such normalized SAR values times the max power rating of the device under test. In this way, we obtain the exposure metrics for 100% talk-time, i.e., without applying source-based time averaging.

A Thevenin model showed in the following figure, featuring a voltage source V_S and real source impedance R_S, is employed in XFDTD to represent the antenna feed.
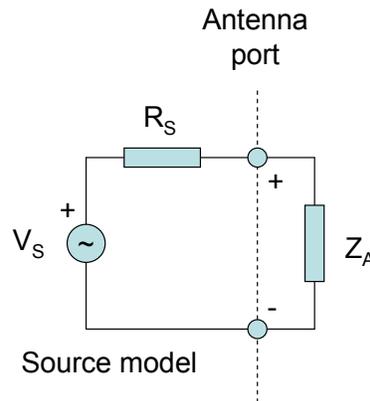
The antenna impedance is $Z_A = R_A + jX_A$. The available power from the source is the one that would be dissipated on the load if perfect the impedance match condition ($Z_A = R_S$) is enforced:

$$P_{av} = \frac{1}{2}\text{Re}\{V_A I_A^*\} = \frac{1}{2}\frac{V_S}{2}\frac{V_S^*}{2R_S} = \frac{|V_S|^2}{8R_S}.$$

The operative condition under which the available power is measured is represented in the following figure. Note that this is the same condition, where the load resistance is represented by a power metering device, used to measure the maximum conducted power from a radio.
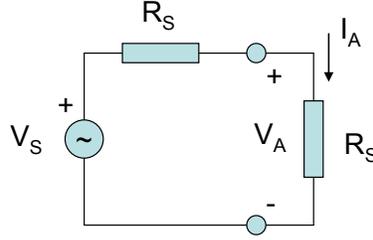
Therefore, it is possible to establish the Thevenin voltage that would be representative of a radio transmitter with maximum rated power P_{max} as follows:

$$P_{max} = \frac{|V_S|^2}{8R_S} \Rightarrow |V_S| = \sqrt{8R_S P_{max}} \ .$$

When the transmitter is connected to an antenna that exhibits an input impedance Z_A, the power radiated is less or equal than the maximum rated power because of two physical mechanisms: energy dissipation in the antenna structure and energy reflection at the antenna port. The first mechanism is due to dielectric and ohmic losses while the second one is due to the impedance mismatch at the antenna port. Neglecting energy dissipation is a mean to introduce a conservative bias in the compliance assessments. In XFDTD, this is accomplished by defining ideal (non lossy) material properties for the radiating structures. Additional conservative bias is introduced by neglecting the mismatch losses. The mismatch loss factor is:

$$\eta = \frac{P_{rad}}{P_{max}} = 1 - |\Gamma|^2 = 1 - \left|\frac{Z_A - R_S}{Z_A + R_S}\right|^2 = \frac{4R_A R_S}{|Z_A + R_S|^2} \ ,$$

where Γ is the reflection coefficient at the antenna port. Therefore, in order to neglect the mismatch loss, in XFDTD the fields are scaled up by a factor $\sqrt{1/\eta}$. This is equivalent to setting $P_{rad} = P_{max}$ and therefore $\Gamma = 0$, which is equivalent to say that there are no mismatch losses and that the maximum rated power of the radio transmitter is radiated.

c) For mobile radios, 50% source-based time averaging is applied by multiplying the SAR values determined at point 12(b) times a 0.5 factor.

REFERENCES

[1] K. S. Yee, "Numerical Solution of Initial Boundary Value Problems Involving Maxwell's Equations in Isotropic Media," *IEEE Transactions on Antennas and*

Propagation, vol. 14, no. 3, 302-307, March 1966.

[2] Z. P. Liao, H. L. Wong, G. P. Yang, and Y. F. Yuan, "A transmitting boundary for transient wave analysis," <u>Scientia Sinica</u>, vol. 28, no. 10, pp 1063-1076, Oct. 1984.

[3] Validation exercise: Mie sphere. Remcom Inc. (enclosed PDF)

Remcom.pdf

[4] NEC-Win PRO ™ v 1.1, Nittany Scientific, Inc., Riverton, UT.

[5] C. M. Collins and M. B. Smith, "Calculations of B1 distribution, SNR, and SAR for a surface coil against an anatomically-accurate human body model," *Magn. Reson. Med*., 45:692-699, 2001. (enclosed TIF)

Collins & Smith.pdf

[6] Martin Siegbahn and Christer Törnevik, "Measurements and FDTD Computations of the IEEE SCC 34 Spherical Bowl and Dipole Antenna," Report to the IEEE Standards Coordinating Committee 34, Sub-Committee 2, 1998. (enclosed PDF)

Ericsson.pdf

[7] C. M. Furse and O. P. Gandhi, "Calculation of electric fields and currents induced in a millimeter-resolution human model at 60 Hz using the FDTD method with a novel time-to-frequency-domain conversion**,"** Antennas and Propagation Society International Symposium, 1996. (enclosed PDF)

Furse & Gandhi.pdf

[8] *The Finite Difference Time Domain Method for Electromagnetics*, Chapter 14.2, by K. S. Kunz and R. J. Luebbers, CRC Press, Boca Raton, Florida, 1993.